UNIVERSITÀ DEGLI STUDI DI PADOVA

Dipartimento di Fisica e Astronomia "Galileo Galilei"

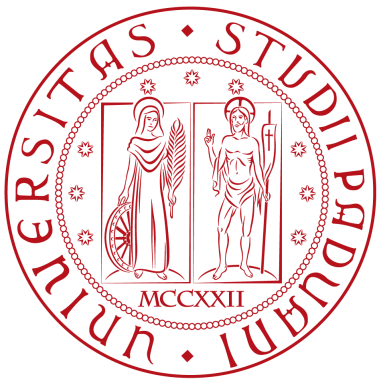

BACHELOR THESIS IN PHYSICS

Characterization of LYSO scintillator screen for future diagnostic of Particle Wakefield Acceleration beams

Laureando/Author:
Oscar CIPOLATO

Relatore/Supervisor:
Prof. Anna Teresa MENEGUZZO

Academic year 2016-2017 – December 2017

UNIVERSITÀ DEGLI STUDI DI PADOVA

Dipartimento di Fisica e Astronomia “Galileo Galilei"

Abstract

Characterization of LYSO scintillator screen for future diagnostic of Particle Wakefield Acceleration beams

by Oscar CIPOLATO

Plasma Wakefield Acceleration is capable of producing high charge bunches with femtosecond pulse duration. Novel diagnostic techniques for the charge spatial distribution of beam bunches are being investigated for the FLASH-Forward project at DESY. The foreseen diagnostic setup with high spatial resolution is based on coated scintillator screens since they can reflect the laser and be used for the electron beam diagnostics. For this purpose, tests for preliminary characterization and for the evaluation of damage threshold of LYSO-type scintillator screens were performed.

Caratterizzazione di uno schermo scintillatore LYSO per future diagnostiche di fasci prodotti da PWFA

di Oscar CIPOLATO

L’accelerazione al plasma (PWA) è in grado di produrre fasci di particelle con carica elevata e durata del pacchetto dell’ordine dei femtosecondi. Nuove tecniche di diagnostica per i fasci di particelle vengono studiate nel progetto FLASHForward a DESY. Il prospettato sistema di diagnostica con elevata risoluzione spaziale è basato su schermi scintillatori in quanto possono riflettere fasci laser e possono essere utilizzati per la diagnostica del fascio di elettroni. Per questo motivo, test per la caratterizzazione e la quantificazione della soglia di danno di uno scintillatore di tipo LYSO è stato svolto.

Acknowledgements

I want to thank all the people who helped me along the period of my thesis. First my supervisor at DESY **Pardis Niknejadi**, without whom this work would have been impossible. Her guidance and suggestions were very precious. Special thanks to **Kristjan Poder** for his help during the experimental sessions. Last but not least, I'd like to thank my supervisor **Anna Teresa Meneguzzo**, always ready to help me and to support me along my thesis work.

I am grateful for the opportunity to have spent the period of my thesis work within the Desy Summer Student program and to professors **Fabio Zwirner** and **Marco Zanetti** for the support to my application.

Contents

Acknowledgements **v**

1 Introduction **1**
1.1 Introduction and motivations 1
1.2 Structure of this Thesis 2

2 Theoretical introduction **3**
2.1 Theory of pulsed lasers 3
2.1.1 Wave equation and Gaussian beams 3
2.1.2 Gaussian beam optics 5
2.2 Plasma wakefield acceleration 6

3 Experiment and experimental setup **11**
3.1 Scintillator screen 11
3.2 Ti:Sapphire laser 12
3.3 Method of beam characterization 13
3.3.1 Beam energy measurement 14
3.3.2 Beam spot size measurement 14
3.4 Final setup 14

4 Experimental results and analysis **17**
4.1 Experimental results and analysis 17
4.2 Beam energy 17
4.2.1 Calibration of image with calorimeter 17
4.2.2 Energy measurements 20
4.3 Beam spot size 20
4.4 Peak intensity calculated 22
4.5 Fluence calculated 22
4.6 Observed Damage 22

5 Future plans and conclusions **25**
5.1 Fine tunning the setup and next steps 25
5.2 Conclusion 25

Bibliography **27**

Chapter 1

Introduction

1.1 Introduction and motivations

High-energy and high-quality particle beams have proven extremely useful in the modern-day science: they are used in colliders for research in particle physics, in free-electron lasers as light sources and in inverse Compton scattering sources for the production of X-ray or gamma-ray beams used to analyze atoms, molecules and material properties. To produce beams with higher energy than the currently available ones while preserving their quality, new particle accelerator technologies must be explored and developed. Plasma wakefield acceleration (PWA) is one of the most promising techniques that can be used in future colliders and light sources. It is able to achieve much greater accelerating gradients and produce much shorter beams than the conventional accelerators. Traditional accelerating structures are made of metal (normal or super-conductive). The properties of the materials impose a limit to the accelerating gradient due to the breakdown of the accelerating structure walls at high fields [1]. The “accelerating structures" in PWA is the plasma, a material which is not “damageable", therefore this acceleration technique doesn’t exhibit the same limitations. The highest accelerating gradient achievable in conventional RF cavities is around 0.1 GeV/m, while in PWA accelerating gradients on the order of 10-100 GeV/m can be achieved [2].

Plasma acceleration was first proposed by T. Tajima and J. Dawson in 1979 [3]: in this scheme a high intensity laser pulse is shot into the plasma, forming density modulations where particles are accelerated. However, laser and beam technologies were not as advanced as today at the time. During the following years, parallel development of laser and beam technologies occurred. In the recent years, plasma acceleration has been able to produce desirable high-quality electron beams [4], [5], [6]. However, characterization of the highly transient wakefield structure and the short electron pulses produced by these wakes are challenging. Novel diagnostic techniques are under investigation at several different PWA facilities including at DESY for the FLASHForward project: FLASHForward is a project at Free electron LASer in Hamburg (FLASH) facility that seeks to investigate PWA and the correlation between the electron bunch properties and the driver beam parameters [7]. Coated scintillator screens that can reflect the laser and be used for the electron beam diagnostics are needed in planned diagnostic setup with high spatial

resolution. For this purpose, a LYSO-type scintillator screen has been characterized and its laser damage threshold has been quantified. That is what I investigated, studied and worked for in my thesis within the FLASHForward team at DESY.

1.2 Structure of this Thesis

The structure of this thesis is a follows: in chapter 2 a brief theoretical introduction about lasers and plasma acceleration will be given. The formulas used in this work will be presented here. In chapter 3 the experimental setup will be presented, while in chapter 4 the experimental method will be explained and the experimental results given. In chapter 5 conclusions and final considerations are given.

Chapter 2

Theoretical introduction

2.1 Theory of pulsed lasers

Lasers that meet light in the form of optical pulses instead of a continuous mode are referred to as pulsed lasers. Depending on the characteristics of the laser pulses (such as energy, duration, wavelength and repetition rate) different methods of pulse generation are used. Pulses with durations in the picosecond or femtosecond regime are typically generated by means of *mode-locked* lasers. For high pulse energies, *regenerative amplifiers* are also utilized.

High intensity pulsed lasers are used in plasma chambers to ionize the gas in order to form the plasma, to induce the charge density modulation and to accelerate the produced electron beam. The laser pulse parameters, such as energy [8], chirp [9] and shape [10], govern the properties of the electron beam accelerated in the plasma. The theory and the properties of pulsed lasers are shortly reported in the following paragraphs.

2.1.1 Wave equation and Gaussian beams

Electric and magnetic fields must obey Maxwell equations:

$$\nabla \cdot \vec{E} = \frac{\rho}{\epsilon}, \qquad \nabla \cdot \vec{B} = 0,$$
$$\nabla \times \vec{E} = -\frac{\partial \vec{B}}{\partial t}, \qquad \nabla \times \vec{B} = \mu \vec{j} + \frac{n^2}{c^2}\frac{\partial \vec{E}}{\partial t},$$

where $\vec{E}$ is the electric field, $\vec{B}$ is the magnetic field, c is the speed of light, n the refractive index of the propagating material, ρ is the charge density, $\vec{j}$ is the current density, μ and ϵ are respectively the permeability and the permittivity of the propagating material. If charge and current density are identically null, Maxwell equations yield to the wave equation

$$\nabla^2 \vec{E} - \frac{1}{v^2}\frac{\partial^2 \vec{E}}{\partial t^2} = 0, \tag{2.1}$$

where $v = \frac{c}{n}$ is the group velocity. We restrict ourself to the electric field, however the previous equation is valid for both $\vec{E}$ and $\vec{B}$, therefore the following statements are also valid for $\vec{B}$. A solution of 2.1 is given by the real part of

the following equation:

$$\vec{E}(\vec{x},t) = \vec{E}_A(\vec{x},t)e^{-i(\omega_0 t - \vec{k}\cdot\vec{x}+\phi(t))}\,, \tag{2.2}$$

where $\vec{E}_A(\vec{x},t)$ is the amplitude function. The wave oscillates with the frequency ω_0, while the wave vector $\vec{k}$ defines the propagating direction and its module is related to the wavelength λ by the relation $|\vec{k}| = \frac{2\pi}{\lambda}$. Another important parameter of the beam is the intensity, defined as the power over area. The electric field and the intensity are correlated:

$$I(\vec{x},t) \propto |\vec{E}_A(\vec{x},t)|\,. \tag{2.3}$$

In first approximation, the electric field is separated into time and spatial domain:

$$\vec{E}_A(\vec{x},t) = \vec{E}_x(\vec{x}) \cdot E_t(t)\,. \tag{2.4}$$

Therefore, we can treat the spatial component and the temporal component of the amplitude separately.

In an isotropic space, the electric and magnetic fields are transverse to the direction of propagation and the waveforms are called *transverse electric and magnetic modes* (TEM) with indices (m,n). The basic solution of the wave function is called TEM_{00} mode or *Gaussian principal mode*:

$$\vec{E}_x(\vec{x}) = \vec{E}_0 \frac{\omega_0}{\omega(z)} e^{-\frac{x^2+y^2}{\omega(z)^2}} e^{-ik\frac{x^2+y^2}{2R(z)}} e^{i\phi(z)}\,. \tag{2.5}$$

The beam radius ω is defined as the distance from the propagating axis where the electric field drops by a factor $\frac{1}{e}$ and, consequently, where the power drops by a factor $\frac{1}{e^2}$. In contrast to ray optics, the minimal spot is not infinitely small, but has a finite radius ω_0, the beam waist. The beam radius $w(z)$ at a certain distance z from the focus point is given by the following formula:

$$w(z) = w_0 \sqrt{1 + \left(\frac{z}{z_R}\right)^2}\,, \tag{2.6}$$

where z_R is the Rayleigh length defined as:

$$z_R = \frac{\pi w_0^2}{\lambda}\,, \tag{2.7}$$

where λ is the wavelength. At a distance of one Rayleigh length the spot size is $\sqrt{2}\omega_0$; in the region where $z < z_R$ the wavefront is parallel to the xy plane.

The temporal part of the solution of the wave function is

$$E_t(t) = E_A(t)e^{-i(\omega_0 t+\phi(t))}\,, \tag{2.8}$$

where $E_A(t)$ is a temporal envelope function. The Gaussian function is typically assumed as a good approximation in laser beams:

$$E_A(t) = E_0 e^{-\frac{t^2}{\tau^2}}, \tag{2.9}$$

where τ is the time at which the electric field drops by the factor $\frac{1}{e}$. If we assume the Gaussian shape for the temporal solution of the wave function, we can evaluate the peak intensity of the laser pulse. The power of a pulse with length σ_t can be calculated from the following formula:

$$P_0 = \frac{E}{\sqrt{2\pi}\sigma_t}. \tag{2.10}$$

The peak intensity $I(z)$ can be calculated given the power of the beam and its waist:

$$I(z) = \frac{2P_0}{\pi w^2(z)} = \frac{2P_0}{\pi w_0^2} \frac{1}{1 + \left(\frac{z}{z_R}\right)^2}. \tag{2.11}$$

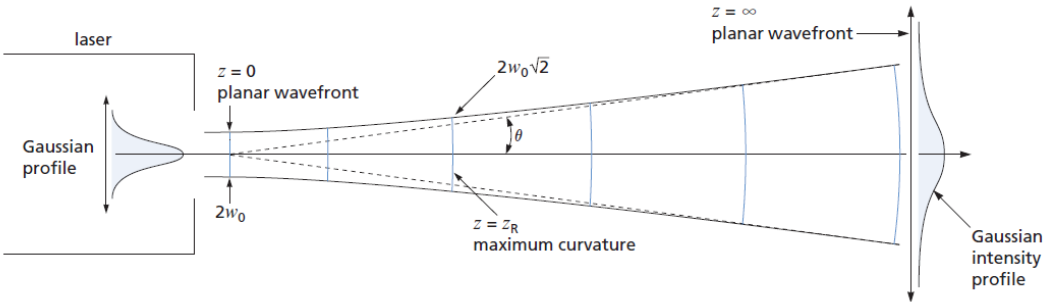

FIGURE 2.1: Change in wavefront radius with propagation distance for Gaussian beam lasers. (Illustration from *CVI Laser Optics*)

2.1.2 Gaussian beam optics

Once the laser pulse is generated, it is manipulated by lenses and mirrors, e.g. lenses are used in order to focus or collimate the beam. The laser pulses need to be focused onto a camera or on a target, such as gas targets for ionization or a scintillator screen. Therefore, understanding how a Gaussian beam propagates through optics is necessary, as ray optics cannot describe the propagation through focusing optics fully because the focus point isn't indefinitely small. The resulting spot size w'_0 is given by

$$w'_0 = M w_0, \tag{2.12}$$

where the magnification M is

$$M = \frac{M_r}{\sqrt{1+r^2}}, \tag{2.13}$$

with

$$M_r = |\frac{f}{z-f}|, \tag{2.14}$$

and

$$r = \frac{z_R}{z-f}. \tag{2.15}$$

In this work, manipulation of the beam is mainly used to focus a collimated beam, so when the position of the beam waist is at the entrance of the lens, which is $z = 0$. This leads to $M_r = 1$ and $r = \frac{z_R}{f}$. Another valid approximation is $z_R \gg f$, since the beam is collimated. Therefore, when using a Gaussian beam, the change of the beam waist after entering a lens of focal length f is given by the following formula:

$$w_f = \frac{\lambda f}{\pi w_0}, \tag{2.16}$$

where w_0 is the initial beam waist and w_f is the beam waist after entering the lens.

2.2 Plasma wakefield acceleration

In the following section, the fundamentals of plasma wakefield acceleration are derived and summarized from [11].

A plasma is a state of matter in which part or all of the electrons and nuclei are not bonded together. Unlike the other three states of matter – gas, liquid, and solid – under normal condition, plasma does not exist on Earth's surface. In order to accelerate particles in plasma, we first need to create the plasma. Plasma can be created from the interaction of high-intensity lasers and matter. When a high-energy laser pulse propagates in a gas target, its electric field influences the atoms in such way that they are ionized, i.e. the electrons are free from the binding Coulomb force of the nuclei. There are mainly three different atomic ionization mechanisms:

- *Direct ionization* and *Multi-photon ionization*: in this mechanism the electric field of the laser pulse is not strong enough to disturb the electric field of the binding Coulomb force. If a single photon has enough energy to overcome the potential barrier we have direct ionization, otherwise multi-photon ionization can occur if multiple photons are needed in order to overcome the binding potential.

- *Tunnel ionization*: if the intensity is high enough, the binding potential is disturbed and a finite Coulomb barrier is given. The electron can get through the barrier via tunnel effect with a certain probability.

- *Barrier suppression ionization*: at very high intensities the binding potential is so strongly disturbed that the electron bound state is above the effective potential.

Particles are accelerated in plasma exploiting the presence of two different charged particle species: electrons and ionized atoms, with the latter way heavier than the first one. When high-intensity lasers or relativistic charged particle bunches traverse the plasma a force is applied on charged particles: the average over time of this force is called *ponderomotive force* and is given by

$$\vec{F}_P = -\frac{e^2}{4m{\omega_0}^2}\nabla|\vec{E}_0|^2\,. \tag{2.17}$$

Since the intensity $I \propto E^2$, the ponderomotive force is proportional to the gradient of the intensity. The ponderomotive force is proportional to the square of the charge, therefore repels charged particles of both signs towards the lower intensities. In the case of a Gaussian beam, the force repels the charges sideways. Due to the ponderomotive force, the electrons are driven away from the driver, while the ions are not affected by it as they are heavier. In such way, regions with high charge density are created and strong electric fields are formed. When the driver beam causes total separation of the electrons and ion charges, maximum acceleration can occur: this regime is non-linear and the cavity that is formed in the plasma that can trap and accelerate charged particles is called *bubble*. The wakefield and the resultant bubble can be produced by high power short pulse lasers or by highly relativistic particle beams. In Laser Wake Field Acceleration (LWFA), plasma wakes are created by a femtosecond-short laser pulse, and in Plasma Wake Field Acceleration (PWFA), a charged beam particle is used to induce the wake.

The bubble shape is sinusoidal in non-relativistic regime and becomes longer in relativistic regime, but the main features of the bubble structure don't change. Looking at the longitudinal electric field we can distinguish two different phases: one phase that can be used to accelerate electrons and one where electron are decelerated. Another distinction can be made looking at the transverse electric field: one phase can be used to focus the electrons, while the other drives the electrons outside the bubble. If the witness bunch is made of positively charged particles the two phases switch function for both longitudinal and transverse phases.These two distinct type of regions are out-of-phase, so if we are trying to accelerate and focus the witness bunch, only one-fourth of the bubble can be used.

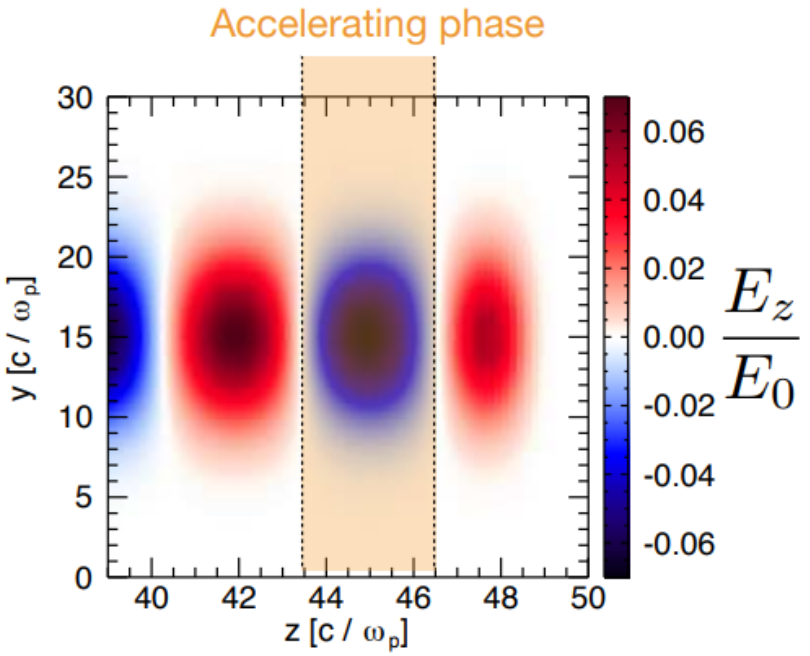

FIGURE 2.2: Longitudinal electric field in plasma wakes: only one region of the bubble can be used to accelerate the witness bunch. (Illustration by Jens Osterhoff)

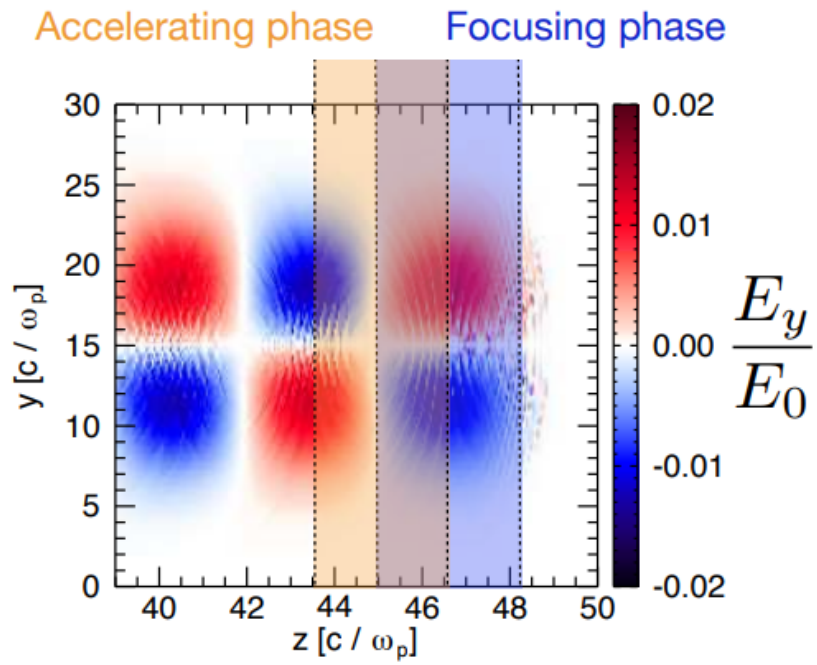

FIGURE 2.3: Transverse electric field in plasma wakes: only one region of the bubble can be used to focus the witness bunch. If we want to accelerate and focus the witness, only one-fourth of the bubble can be used. (Illustration by Jens Osterhoff)

The maximum accelerating field is estimated as follows. The electric field generated by charges shifted by a distance x in a medium with charge density n is $E = nex/\epsilon_0$. The equation of motion

$$F = mad^2x/dt^2 = -eE = -ne^2x/\epsilon_0 \tag{2.18}$$

gives us the oscillation frequency

$$\omega_p^2 = \frac{ne^2}{m\epsilon_0}\,. \tag{2.19}$$

If total charge separation is achieved in plasma, assuming that $x \sim c/\omega_p$, the maximal field is

$$E_{max} \simeq \frac{nec}{\epsilon_0\omega_p}\,. \tag{2.20}$$

Using the practical formula for the plasma frequency in Hz $f_p \simeq 9000n^{1/2}$, where n is in cm^{-3}, we get that the maximum accelerating field in plasma is:

$$eE_{max} \simeq 1\frac{eV}{cm}\cdot n^{1/2}\,. \tag{2.21}$$

This means that we can achieve an accelerating gradient of 1 GeV/cm in a plasma of 10^{18} cm^{-3} density.

To accelerate particles, the witness bunch must be injected at the right longitudinal and transverse position. There are various mechanisms that are under investigation and they can be sorted in two main categories:

- *External injection*: the witness bunch is synchronized with the driver and the energy of the driver is transferred to the witness bunch. The distance between them is such that the witness bunch gets accelerated and focused. The required synchronization between the two bunches is of the order of fs, therefore it is experimentally challenging.

- *Internal injection*: the witness bunch is formed trapping electrons from the plasma into the accelerating region. This can be achieve in different ways: in *self-injection* electron are scattered in the wake, however high shot-to-shot fluctuations in bunch parameter occur due to the statistical nature of this process; in *ionization injection* a two gas species with different ionization threshold are used: the first one is creates the plasma background, whereas the second is responsible for the injected electrons; in *density down-ramp injection* a negative plasma density gradient is exploited to trap electrons in the bubble.

While LWFA has been studied a lot in the last decades, there are some advantages in using a particle bunch to drive the wake instead of using a laser beam, for example:

- the phase velocity of the particle beam traveling through the plasma density is higher than the laser since the particles travel at close to speed of light while the laser propagates at its group velocity, leading to longer acceleration length (1 meter for PWFA, 100 mm for LWFA);

- strongly transverse focusing plasma avoids or reduces expulsion of the beam (unlike the defocusing/diverging laser);
- low dark current as a result of increased wake phase velocity (but this can make trapping charges for the PWFA beam challenging).

For all these reasons PWFA seems very promising and FLASHForward group at DESY is dedicated to studying this technique and its challenges. The initial goal of FLASHForward is to produce high-quality beams. Ultimately, FLASHForward project aims to demonstrate, possibly for the first time, Free-Electron Laser (FEL) gain, by beam driven plasma wakefield accelerated electron beams.

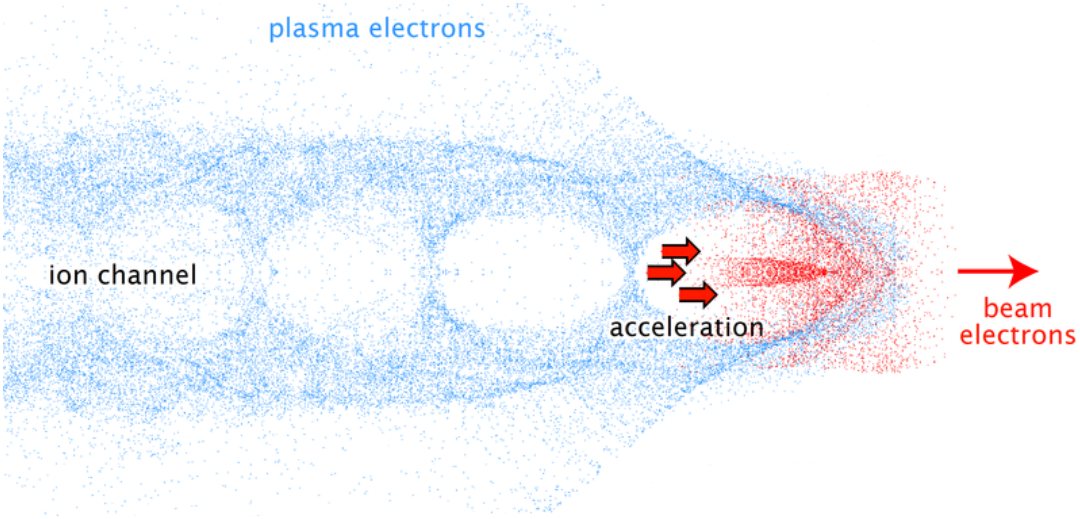

FIGURE 2.4: Illustration of the wake created by an electron bunch traveling inside the plasma. Particles are accelerated in a specific region of the first bubble. (Illustration by Rasmus Ischebeck)

Chapter 3

Experiment and experimental setup

The initial goal of FLASHForward is to produce high-quality electron beams. Ultimately, FLASHForward project aims to demonstrate, possibly for the first time, Free Electron Laser (FEL) gain, by beam driven plasma wakefield accelerated electron beams. As explained in the previous chapter, Particle WakeField Acceleration seems very promising and FLASHForward group at DESY is dedicated to studying this technique and its challenges.

In the FLASHForward project, for the knowledge of the spatial charge distribution of the produced electron beam, scintillator screens are foreseen along the produced beam and then along the laser direction. However, the copropagating laser used for ionizing the gas could cause damage in such screens, compromising the whole experiment. Therefore it is necessary to understand whether the screen will be able to bear high-intensity radiations of the laser.

The scintillator screen characterized in this report will be used as diagnostic in the FLASHForward facility: high energy electron bunches are created copropagating with high-intensity laser and the presence of the laser's electric field may interfere with the diagnostic of the electron bunch. Therefore it is necessary to separate the electron bunch from the laser pulse: the scintillator screen is used to meet this task as it is able to reflect the laser while not blocking the electron bunch. The problem with this setup is that the laser used in FLASHForward has very high intensities, so no material is able to work closer than 10 meters from the beam waist. For this reason, it is necessary to know whether the LYSO screen will be able to function properly at a distance of 10 meters away from the focus of the laser.

3.1 Scintillator screen

The screen that is the candidate for test and diagnostics is a LYSO-type screen with dimension 36.5x29x0.2 mm, CRY019 by Crytur [12]. CRY019 is used because, as pointed out in [13], it has the best spatial resolution between the studied scintillators. LYSO stands for *lutetium-yttrium oxyorthosilicate*, it is an inorganic scintillator widely used because of its high light output and density, quick decay time, excellent energy resolution and it isn't hygroscopic. Its chemical formula is $Lu_{2(1-x)}Y_{2x}SiO_5$. The test screen for the measurement discussed here is 0.2 mm thin CRY019 strip and it was coated by metal and

multilayer dielectric layers to reflect the laser pulse. Only one side of the screen is coated.

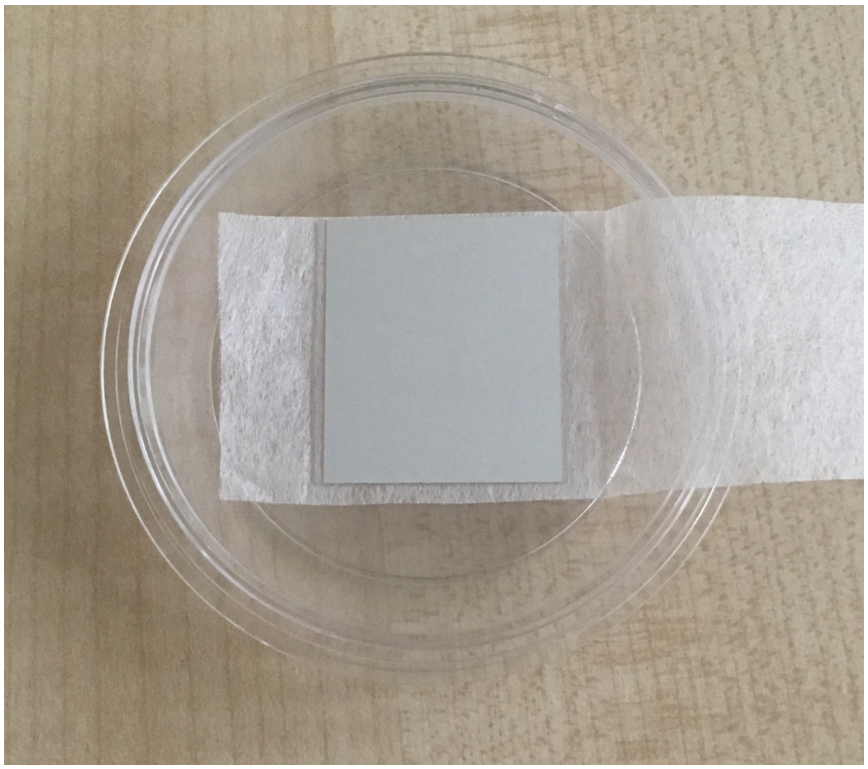

FIGURE 3.1: Photo of a scintillator screen used for diagnostic.

3.2 Ti:Sapphire laser

In the following section, the laser system is summarized from [14]. The laser system is a commercial system from the company Amplitude [15]. A schematic drawing is shown in picture 4.1. The system starts with a fs Ti:Sapphire oscillator, where pulses with a duration of less than 8 fs and a 108 MHz repetition rate are created. It is send to a booster module in order to amplify the pulse and reduce the pulse repetition rate. The pulse is amplified by a multipass amplifier: a gain medium can achieve a limited amount of gain, so in order to achieve a much greater gain we geometrically arrange multiple passes through the gain medium. The repetition rate is reduced using a Pockels cell, a device able to work as a nanosecond shutter. After the booster the beam is stretched in the stretcher, the pulse length is increased in order to decrease the beam intensity. Afterwards the beam is amplified by a multipass and a regenerative amplifier, where the beam passes through the gain medium multiple times, trapped in an optical resonator. After this second amplification the pulse is split in two branches. The first one goes to the air compressor, where the pulse gets compressed to fs length. The second one is amplified in another multipass amplifier and then compressed in a vacuum compressor, because the pulse energy is too high to compress it in air.

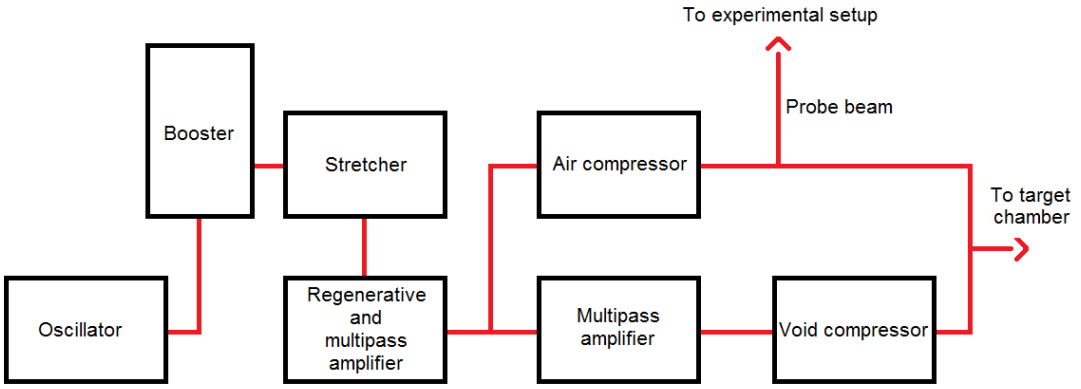

FIGURE 3.2: Schematic drawing of the laser system. The probe beam used in the study of the scintillator screen is the one produced by the air compressor.

The laser used in the FLASHForward experiment is a 25 TW Ti:Sapphire laser. For the test set up described here, the secondary beam of the FLASHForward Ti:Sapphire laser, probe beam, is used. The probe beam is the one produced by the air compressor. The typical properties of the beam used in this experiment are the following:

TABLE 3.1: Probe beam properties.

Wavelength	800 nm
Radius	5 mm
Repetition rate	10 Hz
Energy per pulse	3.5 mJ
Pulse length	25-56 fs

3.3 Method of beam characterization

There are two types of damage that can limit the utility of the LYSO screen: damage due to heat and damage due to intensity. Typically the heat damage is discussed in terms of flux or fluence of the beam J/cm^2 with relatively long durations (nanosecond long). The damage of concern here is the intensity based damage due to short (femtosecond long) pulses. To determine the damage intensity threshold accurately the energy focused, spot size and pulse length at the probe must be carefully measured. Beam duration is measured using GRENOUILLE technique [16]. We assume all pulses have approximately the same length.

3.3.1 Beam energy measurement

As shown in Figure 3.3, beam energy was estimated sending part of the probe beam to a calibrated CCD camera. To this end, a dielectric mirror was put at an angle of 45° with respect to the beam axis: the transmitted beam went to the camera, the reflected beam proceeded to the remaining experimental setup. The intensity recorded by the camera is proportional to the energy of the beam. In order to know the conversion relation given a certain setup, the energy of a set of beams was measured by a calorimeter after the lens focusing on the target and compared to the images recorded by the camera. This data was used as a reference. The camera is equipped with filters in order to avoid saturation and damaging. Gain and distance from the lens focusing on the camera were chosen in order to have a small but not saturated beam image.

3.3.2 Beam spot size measurement

The probe beam initial spot size is around $w_{in} = 50\,\text{mm}$ and the peak intensity is low, approximately on the order of few thousands of W/cm^2. In order to achieve higher intensities and smaller spot sizes, a proper experimental setup must be defined. The following facts were taken into account when defining the experimental setup:

- high intensities are required;
- plano-convex lenses are preferred over biconvex lenses due to lower aberration;
- small z_R compared to the sensibility of screen positioning leads to difficulties in finding the focus;
- limited space for the experimental setup;
- due to its many modes, a Ti:Sapphire laser would have the best intensity profile only at focus.

In the experiment, one plano-convex lens was used to focus the beam. The scintillator screen was put perpendicular to the direction of propagation of the beam, positioned at the focal plane.

In order to measure the beam spot size, a BASLER acA1300-30gm camera was placed in front of the screen forming a small angle with the propagation direction; the beam spot size was measured from the scattered light recorded by the camera.

3.4 Final setup

The final setup is shown in the following image.

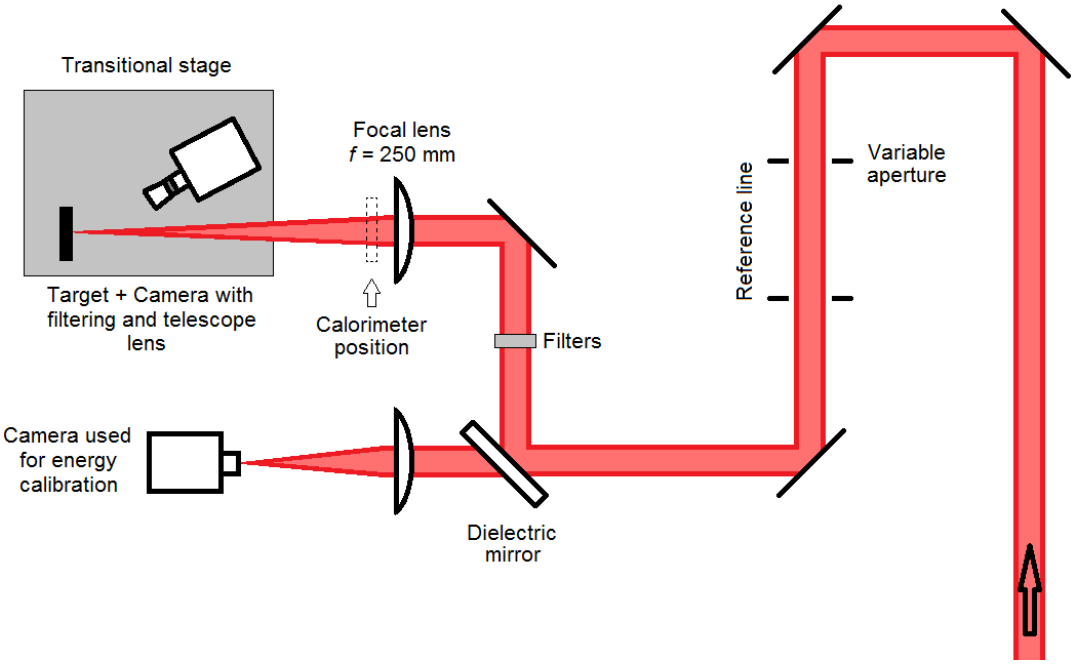

FIGURE 3.3: Experimental setup.

The following optical elements are used:

- ⌀50.8mm broadband mirrors;
- apertures;
- plano-convex lenses: $f = 250$ mm; $f = 100$ mm;
- dielectric mirror BB4-E03 by Thorlabs;
- BASLER acA1300-30gm cameras;
- filters: ND2.0, ND3.0 and ND4.0.

The screen and the camera were mounted on the stage, so the camera didn't need to be refocused every time the screen is moved. The camera is put on the stage and focused on the screen at the beginning of the experiment the focusing is not changed during the experiment to avoid inconsistencies.

Chapter 4

Experimental results and analysis

4.1 Experimental results and analysis

Different beam energy and beam repetitions are used in order to investigate the damage threshold of the scintillator screen as reported in table 4.1.

TABLE 4.1: Experimental beam energy and time of exposure.

Identification number	Filtering	Aperture size	Time of exposure [sec]
1	ND4	Almost closed	60
2	ND4	Half-opened	60
3	ND4	Fully opened	60
4	ND3	Almost closed	120
5	ND3	Fully opened	120
6	ND2	Half-opened	120
7	ND2	Fully opened	120

4.2 Beam energy

4.2.1 Calibration of image with calorimeter

Three data set at different aperture sizes were taken (open aperture, middle size aperture, and small size aperture). Each one has 700 images and 600 energy measurements. The number of images is greater as the camera begins to save data immediately while the calorimeter begins saving data only after a certain threshold is reached, so after removing the obstacle used to block the laser from the beam trajectory: the first image of the beam corresponds to the first energy measurement.

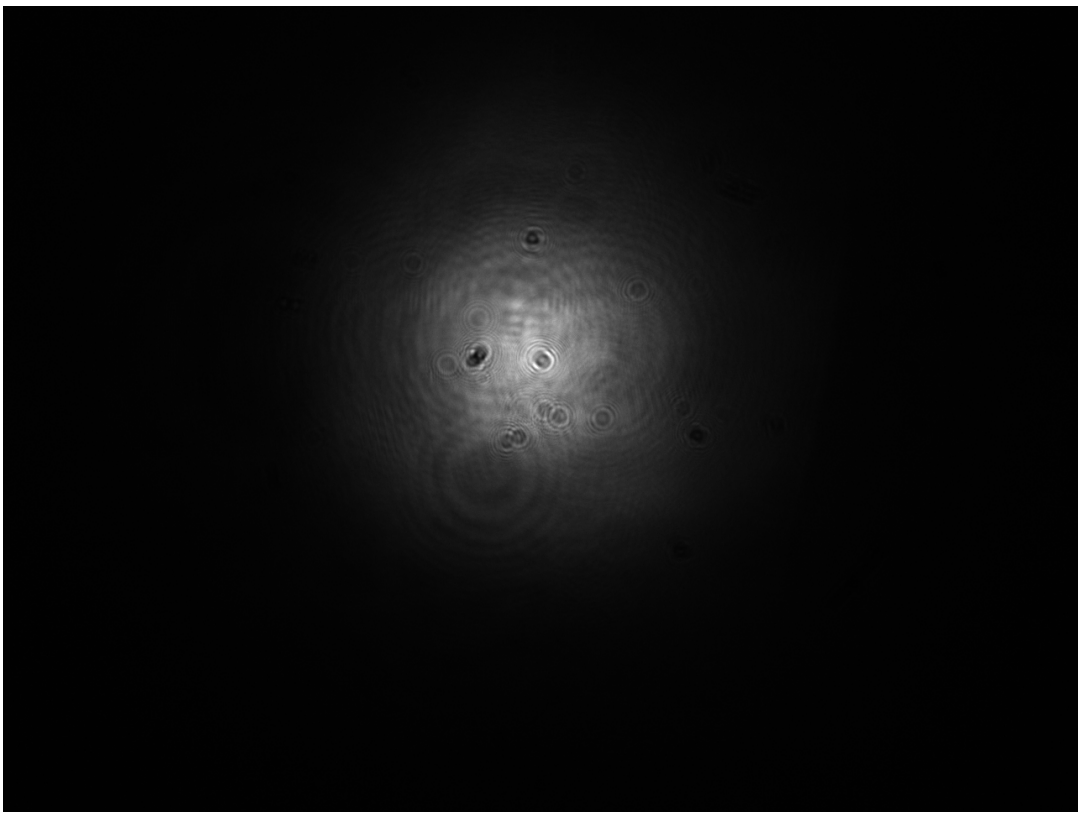

FIGURE 4.1: Image of the beam recorded by the camera. The energy of the beam is proportional to the total intensity recorded by the camera, estimated as the sum of the intensities over all pixels.

The energy of the beam should be proportional to the total intensity recorded by the camera: each pixel records a certain intensity proportional to the number of photons hitting the pixel. Therefore, the total intensity is estimated as the sum of the intensities over all pixels. The conversion between the intensity recorded by the camera (I) and energy (E) is evaluated using a linear fit $I = a + b \cdot E$, one for the data with the open aperture, one for the data with not-fully open apertures.

Additionally, the background must be taken into account which can be evaluated by averaging the intensities on the border of each image, away from the beam, or it can be evaluated by averaging the intensities recorded while the beam was blocked. The first method is preferable when possible as it doesn't take assume that the background doesn't change during the measurements. However, the beam with the open aperture is so large that even along the borders it isn't negligible, as the background evaluated with the first method is much greater than the one evaluated with the second method (while this doesn't happen with middle and small size aperture). The second method is used in such case. The fact that backgrounds evaluated with the second method are compatible regardless of the recording time (it is the same for open, middle and small size aperture, taken at different times) supports

the hypothesis that the background is stable during the measurements and therefore the second method is applicable.

The fact that the beam is so wide that it is not negligible along the borders of the CCD has also some implications on the energy conversion: data taken with the open aperture will have a certain conversion value, as the intensity of the beam is not fully recorded by the camera, while data taken with medium or small size aperture will have another conversion value, as the intensity of the beam is fully recorded by the camera.

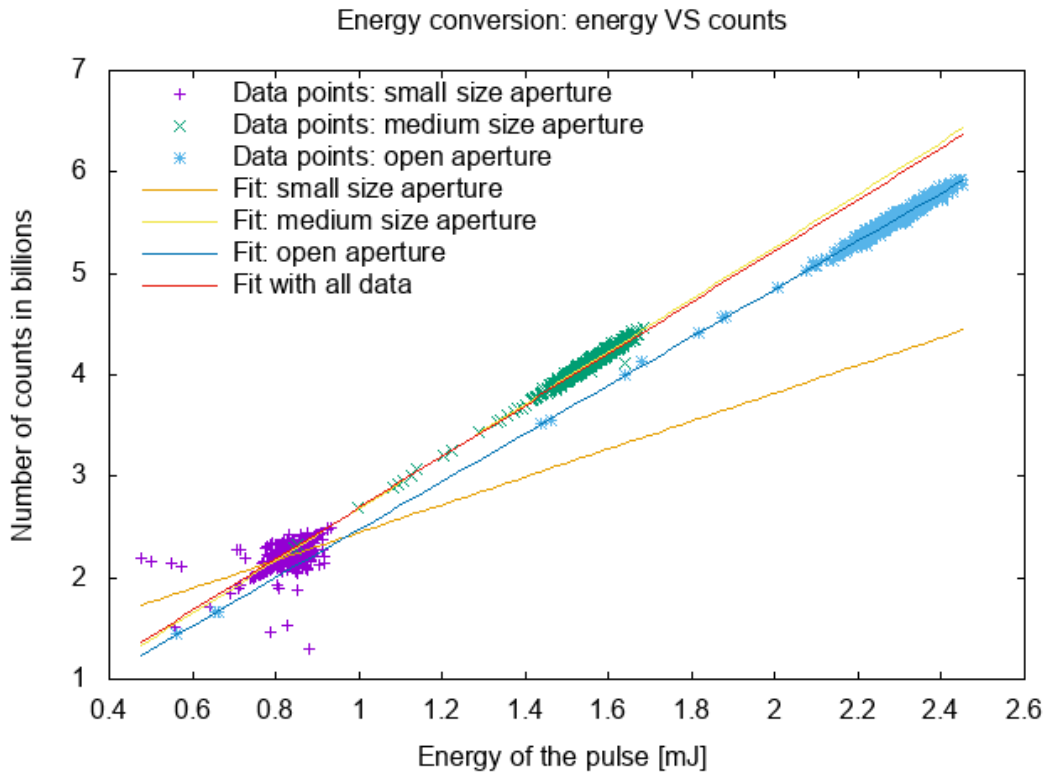

FIGURE 4.2: Energy conversion plot.

As it can be seen in Figure 4.2, data with the open aperture are clearly fitted by other parameters. Thus, using a fit that takes into account all data would be wrong, as it underestimates the energy of the beams taken with the aperture fully open.

TABLE 4.2: $I = a + b \cdot E$ fit parameters.

Parameters	Small-medium aperture size	Open aperture
a [a.u.]	0.10 ± 0.01	0.10 ± 0.01
b [a.u./mJ]	2.582 ± 0.008	2.372 ± 0.005

4.2.2 Energy measurements

Given the conversion values, energy for every setup is evaluated and the results are reported in table 4.3. For a set of 50 images from the energy-related camera, the mean value of the total intensity of a set is used as the estimate of the average beam energy for that particular setup.

TABLE 4.3: Evaluated beam energies.

Identification number	I in billions	Energy [mJ]
1	2.57±0.09	0.96±0.03
2	5.6±0.2	2.13±0.07
3	5.9±0.2	2.45±0.09
4	2.5±0.2	0.94±0.06
5	5.8±0.4	2.4±0.2
6	5.3±0.3	2.02±0.07
7	5.8±0.4	2.4±0.2

4.3 Beam spot size

For every setup, a set of 50 images of the screen hit by the beam with an ND5 filter (or ND6 if needed) was taken: the presence of the filters does not change the beam spot size, but it diminishes the scattered light to the level appropriate for measuring the beam spot size in which the camera is not saturated or damaged. A Gaussian fit is used in order to estimate the beam spot size. The fit is done choosing a range of few pixels around the brightest pixel. The fit is done both vertically and horizontally and the average of the two resulting widths is used as the final estimation, as reported in figure 4.3 and in table 4.4. The presence of the background is managed by adding a constant variable to the Gaussian fit.

In almost all setups in the images two spots were present. This is due to the fact that the screen has two surfaces, with only one reflective, so if the reflective surface is not the closer surface to the laser two spots will be seen. For data analysis, the same spot was always used consistently.

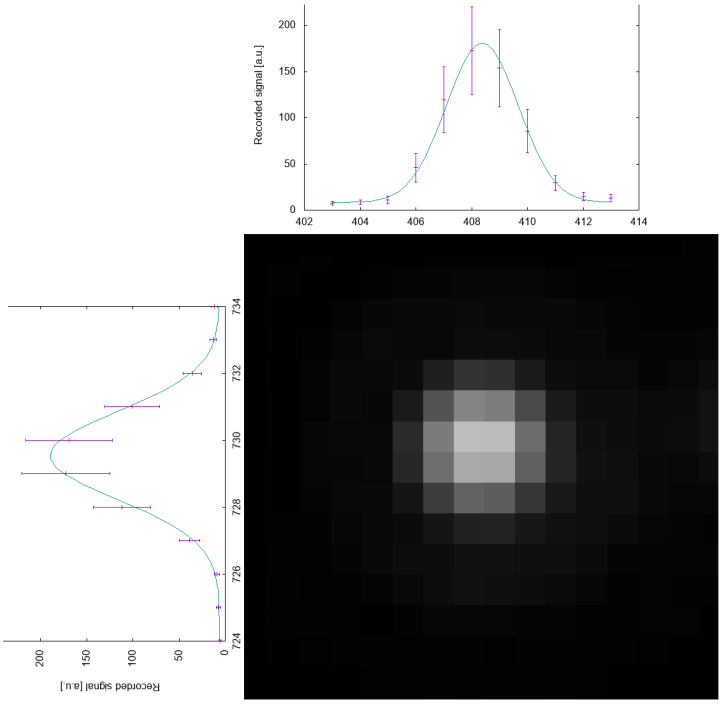

FIGURE 4.3: Spot size and Gaussian fit.

TABLE 4.4: Beam spot sizes.

Identification number	Beam spot size [μm]
1	8.9 ± 0.7
2	11 ± 1
3	8.7 ± 0.3
4	8.9 ± 0.7
5	11.5 ± 0.4
6	12 ± 1
7	11.5 ± 0.4

The resolution of the camera is about 8 μm, which was estimated to be around the beam sizes measured. However changing the aperture should have changed the beam spot size (smaller aperture should have bigger spot sizes for a Gaussian beam after being focused by a lens) but this effect is not seen. Therefore it is possible that the camera resolution was not good enough. In this case, the values obtained would be upper-bound estimates and result in large error bars; consequentially, the obtained intensity values would be lower-bound estimates.

4.4 Peak intensity calculated

High peak intensity is responsible for intensity damage. The beam length, important in this damage mechanism was measured for another experiment on the same optical table to be $\sigma_t = 40 \pm 10$ fs. The results are shown in table 5.1.

TABLE 4.5: Peak intensity.

Identification number	Peak intensity [TW/cm^2]	Relative error
1	0.8 ± 0.1	15 %
2	1.1 ± 0.2	16 %
3	2.0 ± 0.3	13 %
4	8 ± 1	15 %
5	12 ± 2	13 %
6	90 ± 13	15 %
7	116 ± 16	13 %

4.5 Fluence calculated

Fluence is responsible for heat damage to the screen. The results are shown in table 4.6.

TABLE 4.6: Fluence.

Identification number	Fluence [J/cm^2]
1	0.04 ± 0.02
2	0.06 ± 0.04
3	0.10 ± 0.03
4	0.4 ± 0.2
5	0.6 ± 0.2
6	5 ± 2
7	6 ± 2

4.6 Observed Damage

To evaluate the eventual damage of the screen done by the laser, the screen was illuminated by white light before and after the shooting session: if the

beam damaged the screen a white spot of scattered light was anticipated, as see in image 4.4.

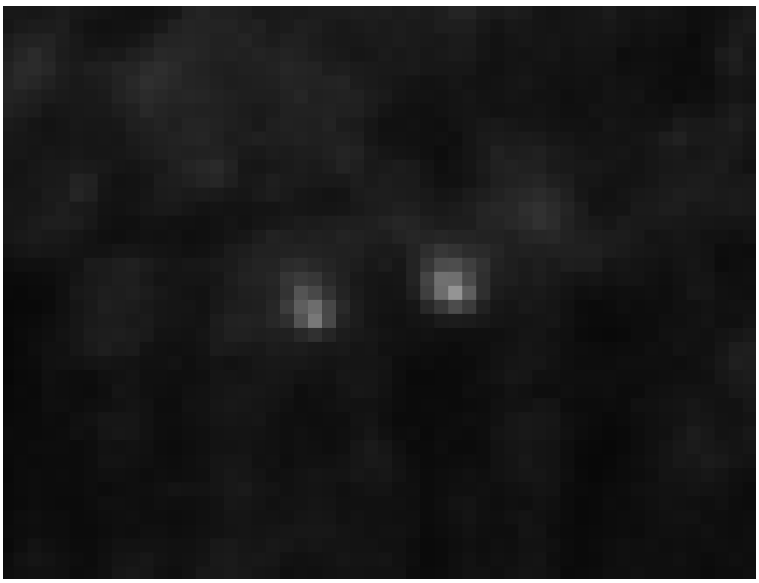

FIGURE 4.4: Damage done after shooting with ND2.

The damage of the screen was determined as follows. An average $\bar{I}$ of the recorded intensity before the shooting session is computed nearby the shot region. If, after the shooting session, the camera registers a peak around the shot region with at least one value of intensity higher than $\bar{I} \pm 3\sigma_I$, the scintillator was considered damaged.

Damage was seen only when shooting laser with ND2 filters.

Chapter 5

Future plans and conclusions

5.1 Fine tunning the setup and next steps

The same setup can be used, after adjustment for better focusing and resolution, for further measurements in the region between 10 and 90 TW/cm^2. Based on what was learned from calculations and setups presented here, the following additional steps can be considered next: changing the aperture size, and using different filter (e.g. using ND1.3).

A possible way to see whether the damage to the screen was due to intensity or heat is by exposing the screen to a few pulses. If any damage is seen in single shot, the damage is caused by the high intensity. If no damage is seen in single shot mode, the damage done by exposing the screen for multiple shoots is due to heat effects.

A microscope lens system can be used on the camera to evaluate more accurately the beam waist.

The setup can also be used to see whether the screen would exhibit back emission. A monochromatic filter for $f = 800$ nm can be put in front of the camera in order to block scattered laser light, if the camera is recording a signal, then the screen is emitting radiation and back emission can be measured.

5.2 Conclusion

From simulation of the foreseen setup, after 10 meters from the beam waist, the FLASHForward laser will have a peak intensity equal to 1.812 TW/cm^2 and a fluence of 0.09084 J/cm^2. From the measurements performed and reported in the previous chapters, the expected foreseen behavior of the screen is reported in table 5.1 and in image 5.1.

TABLE 5.1: Final results.

Exposure time [s]	Peak intensity [TW/cm^2]	LYSO screen response
60	0.8 ± 0.1	–
60	1.1 ± 0.2	–
60	2.0 ± 0.3	–
120	8 ± 1	–
120	12 ± 2	–
120	90 ± 13	Damage
120	116 ± 16	Damage

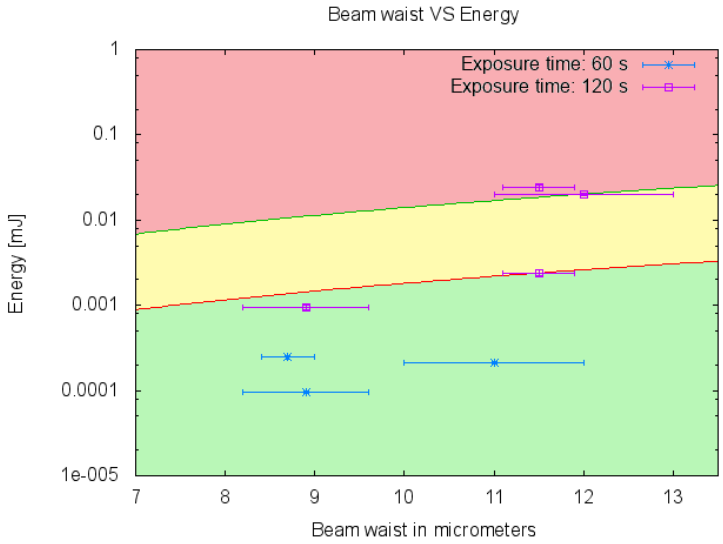

FIGURE 5.1: Energy vs. Beam width (at 40 fs): beam in red area is going to damage the screen; yellow area must be investigated; beam in green area is not going to damage the screen.

Therefore, at distance 10-12 meters from the focus of the ionizing laser, there will not be any heat damage on the screen. With the current data, intensity damage can not be fully ruled out and a second measurement after fine tunning the designed set up is needed.

Bibliography

[1] N. A. Solyak. "Gradient limitations in room temperature and superconducting acceleration structures". In: *AIP Conference Proceedings*. 2009. DOI: 10.1063/1.3080933.

[2] W. P. Leemans et al. "GeV electron beams from a centimetre-scale accelerator". In: *Nature Physics* (2006). ISSN: 1745-2473. DOI: 10.1038/nphys418.

[3] T. Tajima and J. M. Dawson. "Laser electron accelerator". In: *Physical Review Letters* (1979). ISSN: 00319007. DOI: 10.1103/PhysRevLett.43.267.

[4] C. G. R. Geddes et al. "High-quality electron beams from a laser wakefield accelerator using plasma-channel guiding". In: *Nature* (2004). ISSN: 0028-0836. DOI: 10.1038/nature02900.

[5] J. Faure et al. "A laser–plasma accelerator producing monoenergetic electron beams". In: *Nature* (2004). ISSN: 0028-0836. DOI: 10.1038/nature02963.

[6] S. P D Mangles et al. "On the stability of laser wakefield electron accelerators in the monoenergetic regime". In: *Physics of Plasmas*. 2007. ISBN: 1070-664X. DOI: 10.1063/1.2436481.

[7] A. Aschikhin et al. "The FLASHForward facility at DESY". In: *Nuclear Instruments and Methods in Physics Research, Section A: Accelerators, Spectrometers, Detectors and Associated Equipment* (2016). ISSN: 01689002. DOI: 10.1016/j.nima.2015.10.005. arXiv: 1508.03192.

[8] S. P. D. Mangles et al. "Monoenergetic beams of relativistic electrons from intense laser–plasma interactions". In: *Nature* (2004). ISSN: 0028-0836. DOI: 10.1038/nature02939.

[9] A. Popp et al. "All-optical steering of laser-wakefield-accelerated electron beams". In: *Physical Review Letters* (2010). ISSN: 00319007. DOI: 10.1103/PhysRevLett.105.215001.

[10] W. P. Leemans et al. "Electron-yield enhancement in a laser-wakefield accelerator driven by asymmetric laser pulses". In: *Physical Review Letters* (2002). ISSN: 00319007. DOI: 10.1103/PhysRevLett.89.174802.

[11] Andrei Seryi.

[12] CRYTUR. "CRY019 characteristics". In: *https://www.crytur.cz/materials/cry-19/* (2017).

[13] G. Kube et al. "Inorganic scintillators for particle beam profile diagnostics of highly brilliant and highly energetic electron beams". In: *Proceedings of IPAC2012, New Orleans, Lousiana, USA* (2012).

[14] Jan-Niclas Gruse. "Calibration of Laser Diagnostic for Laser Plasma-Wakefield Acceleration". In: *Master's Thesis at Hamburg University* (2016).

[15] Amplitude Technologies. *Pulsar - 10 Hz Femtosecond system*. 2016.

[16] Rick Trebino et al. "Measuring ultrashort laser pulses in the time-frequency domain using frequency-resolved optical gating". In: *Review of Scientific Instruments* (1997). ISSN: 0034-6748. DOI: 10.1063/1.1148286.